

# Accelerating Large-Scale Dataset Distillation via Exploration–Exploitation Optimization

Muhammad J. Alahmadi<sup>1,2</sup> Peng Gao<sup>1</sup> Feiyi Wang<sup>3</sup> Dongkuan (DK) Xu<sup>1</sup>

<sup>1</sup>North Carolina State University <sup>2</sup>King Abdulaziz University

{mjalahma, pgao5, dxu27}@ncsu.edu fwang@ornl.gov

<sup>3</sup>Oak Ridge National Laboratory

mjalahmadi@kau.edu.sa

## Abstract

Dataset distillation compresses the original data into compact synthetic datasets, reducing training time and storage while retaining model performance, enabling deployment under limited resources. Although recent decoupling-based distillation methods enable dataset distillation at large-scale, they continue to face an efficiency gap: optimization-based decoupling methods achieve higher accuracy but demand intensive computation, whereas optimization-free decoupling methods are efficient but sacrifice accuracy. To overcome this trade-off, we propose *Exploration–Exploitation Distillation (E<sup>2</sup>D)*, a simple, practical method that minimizes redundant computation through an efficient pipeline that begins with full-image initialization to preserve semantic integrity and feature diversity. It then uses a two-phase optimization strategy: an exploration phase that performs uniform updates and identifies high-loss regions, and an exploitation phase that focuses updates on these regions to accelerate convergence. We evaluate E<sup>2</sup>D on large-scale benchmarks, surpassing the state-of-the-art on ImageNet-1K while being 18× faster, and on ImageNet-21K, our method substantially improves accuracy while remaining 4.3× faster. These results demonstrate that targeted, redundancy-reducing updates, rather than brute-force optimization, bridge the gap between accuracy and efficiency in large-scale dataset distillation. Code is available at <https://github.com/ncsu-dk-lab>.

## 1. Introduction

Dataset distillation, also known as dataset condensation, aims to distill the original data into compact synthetic datasets that retain the key information of the original data while being orders of magnitude smaller [2, 33, 34, 42]. Distilled datasets train models faster and require less storage, enabling adaptability and real-world deployment under tight time and resource budgets [27, 34, 39]. Despite recent advances, dataset distillation remains constrained by high

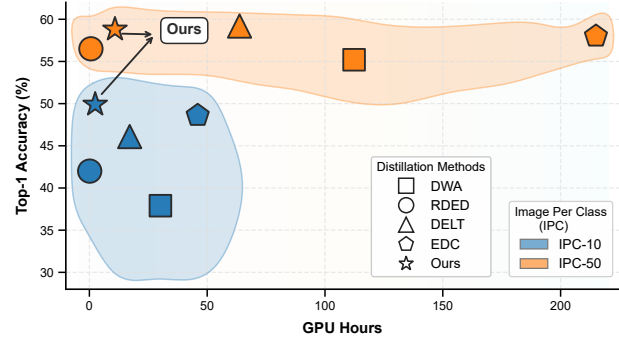


Figure 1. Comparison of Top-1 accuracy and synthesis time on ImageNet-1K using ResNet-18 for various dataset distillation methods at IPC 10 and IPC 50. Synthesis time is measured on a single RTX A6000 GPU. Our method converges substantially faster and achieves the highest accuracy, leading to the best accuracy–efficiency trade-off.

computational cost, with the most common bi-level distillation methods requiring days to synthesize even moderately sized datasets (e.g., CIFAR-100) [12, 38, 42].

In response, a line of work on efficiency and scalability introduced the *decoupled paradigm* [1, 37], which separates model training from synthetic data optimization to avoid costly bi-level updates. This paradigm emphasizes the generation of soft labels to provide richer supervision, transferring much of the computational burden from optimization to label generation, as one study emphasizes “a label is worth a thousand images” [20, 35]. Building on this trend, RDED [29] advances the decoupled paradigm toward an optimization-free approach, eliminating iterative updates by directly extracting and recombining representative patches from real images, reducing synthesis time from hours to minutes.

Nevertheless, the drive toward faster distillation has not overcome the accuracy–efficiency trade-off. Optimization-free methods are fast but lose accuracy, since the teacher only guides patch selection without optimizing the synthetic data. In contrast, optimization-based methods typically achieve higher accuracy, especially when combined with optimization-free strategies as an initialization step [25, 32], but remain computationally expensive. For instance,

EDC [25], a recent dataset distillation method, requires over **200 GPU hours** to distill ImageNet-1K at 50 IPC. Our work aims to bridge this gap by asking two key questions.

- **Q1:** How can we accelerate decoupling-based distillation to narrow the accuracy–efficiency gap?
- **Q2:** Building on the efficiency focus, we ask whether decoupling-based distillation can reach its best accuracy early, such that further optimization not only adds cost but also degrade performance, challenging the assumption that more optimization always helps?

We attribute inefficiency in recent decoupling-based dataset distillation methods to redundancy which we argue stems from two main sources: similar patches generated during initialization, and repeated low-value updates during optimization. Existing methods propagate redundancy by applying uniform gradient updates across all regions, regardless of their contribution to loss reduction. This uniform treatment [7, 25, 37] inflates computation without improving representational quality. Unlike prior work that focuses only on diversity [7, 24, 26], we explicitly *reduce redundancy*, aligning efficiency and diversity to steer dataset distillation away from brute-force optimization toward leaner, more focused updates.

To address **Q1**, we revisit patch-based initialization adopted in prior works [25, 26, 29]. This mechanism often produces clusters of similar patches, which reduces diversity and limits the representational coverage of the synthetic dataset, particularly when multiple patches originate from the same image, as shown in Fig. 3. Moreover, compact patch representations can distort features, compromising the quality of the synthetic data [44]. We instead use full-size image initialization, which ensures better initial representations, reducing the need for extensive optimization. Remarkably, this simple change produces distilled data that already matches the accuracy of state-of-the-art methods before any optimization, substantially narrowing the efficiency–accuracy gap.

Next, we propose a two-phase optimization strategy that reduces the redundant uniform updates of prior works. Rather than treating all regions in the synthetic data as equally valuable, the **exploration** phase broadly updates diverse regions to ensure coverage, before the **exploitation** phase concentrates updates on high-loss regions that provide stronger learning signals. This accelerates convergence and, with an accelerated student training schedule, delivers up to  $20\times$  efficiency gains (Fig. 1).

Turning to **Q2**, we make the counter-traditional observation that more optimization is not always beneficial. Prolonged updates tend to reinforce redundant global dataset statistics while eroding both diversity and fine-grained features inherent in the original dataset. In contrast, our approach demonstrates that a focused optimization strategy can yield higher-quality distilled datasets with fewer

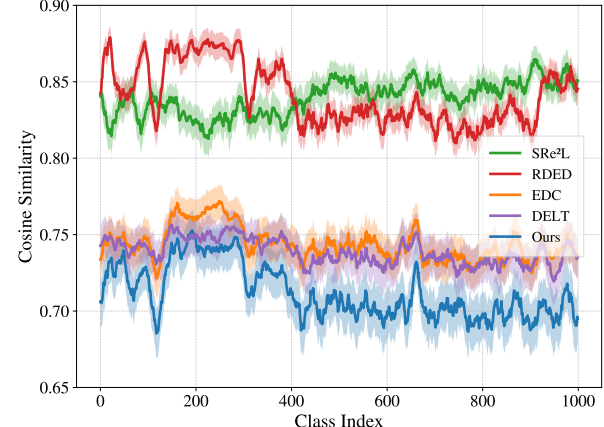


Figure 2. Semantic cosine similarity across ImageNet-1K classes at IPC 50 using a ResNet-18 teacher. Lower values indicate greater diversity and reduced redundancy; our method consistently achieves the lowest similarity.

optimization steps. As illustrated in Fig. 2, our method achieves consistently lower semantic cosine similarity across ImageNet-1K classes, indicating richer diversity. At the same time, it achieves state-of-the-art accuracy, reaching peak ImageNet-1K performance with  $\approx 10\times$  fewer optimization steps than EDC (Fig. 1). This challenges the conventional assumption that longer optimization is always beneficial and highlights the importance of efficient optimization.

Our main contributions are:

1. We identify redundancy as a key inefficiency in recent decoupling-based dataset distillation. It arises from patch-based initialization, where similar crops dominate, and uniform optimization that ignores regional importance. While prior work assumes more optimization improves data, we find excessive updates amplify redundancy and degrade quality, reframing dataset distillation as an efficiency-driven, diversity-aligned process.
2. We propose the Exploration–Exploitation Distillation method (E<sup>2</sup>D) which departs from prior uniform optimization methods by integrating full-image initialization to preserve semantic integrity and diversity with a novel two-phase optimization strategy that identifies high-loss regions and concentrates updates there to reduce redundancy and accelerate convergence.
3. Extensive experiments validate the effectiveness of E<sup>2</sup>D on large-scale benchmarks. On ImageNet-1K, it surpasses state-of-the-art methods while reducing synthesis time by up to **18x**. On ImageNet-21K, it yields accuracy gains of up to **+9.6%** while remaining **4.3x** faster. These results show that E<sup>2</sup>D achieves a superior balance between accuracy and computational cost, making it a practical solution for large-scale dataset distillation.

## 2. Related Work

**Bi-Level Optimization Distillation.** Early dataset distillation methods often adopt *bi-level optimization*, where synthetic data updates are aligned with updates of models trained on the original dataset, in a batch-by-batch manner. Matching strategies include *gradient matching* [12, 38, 42], *trajectory matching* [2, 4], and *distribution matching* [14, 33, 39, 41, 45]. While distribution matching avoids costly bi-level optimization, it typically underperforms gradient or trajectory matching. To address this trade-off, Zhang et al. [38] accelerate gradient-based optimization through early-model augmentation and parameter perturbation. DREAM [15] accelerates optimization by matching only representative images from the original dataset. TESLA [4] extends trajectory matching to ImageNet-1K with memory reduction and soft labels, but remains resource-intensive. Overall, these methods achieve strong alignment but struggle to scale beyond small datasets.

**Decoupled-based Distillation.** To improve scalability, decoupled-based approaches separate model training from synthetic data optimization. SRe<sup>2</sup>L [37] introduces a three-stage pipeline: *Squeeze* (pretrain with Batch Normalization (BN) statistics), *Recover* (independent optimization of synthetic data with global (BN) alignment), and *Relabel* (assign soft labels via a teacher model). CDA [36] scales to ImageNet-21K and further enhances performance with curriculum-based augmentation. RDED [29] follows a similar decoupled approach but removes the optimization stage, yielding several-fold efficiency improvement by selecting teacher-guided patches that balance diversity and realism [13].

**Diversity in Decoupled-based Distillation.** Several works address the limited diversity of global-statistics alignment in the decoupled-based distillation. DWA [7] promotes diversity by dynamically adjusting teacher weights and separating BN mean and variance terms to strengthen variance alignment. G-VBSM [24] expands diversity by incorporating multiple backbones, layers, and statistics. More recently, EDC [25] builds on this framework to enhance both performance and efficiency through pipeline refinements across the distillation process. DELT [26] enhances diversity at the IPC level by assigning different optimization depths to each synthetic image, producing image-level variation to reduce uniformity in decoupled distillation.

**Generative Distillation.** A parallel line of work explores generative approaches such as diffusion-based distillation [8, 19, 28, 44] and GAN-guided synthesis [3, 40, 43] which shift from matching updates to training generative models that output synthetic data. However, they are orthogonal to optimization-based methods, as their generative outputs can be used as initialization for further refinement.

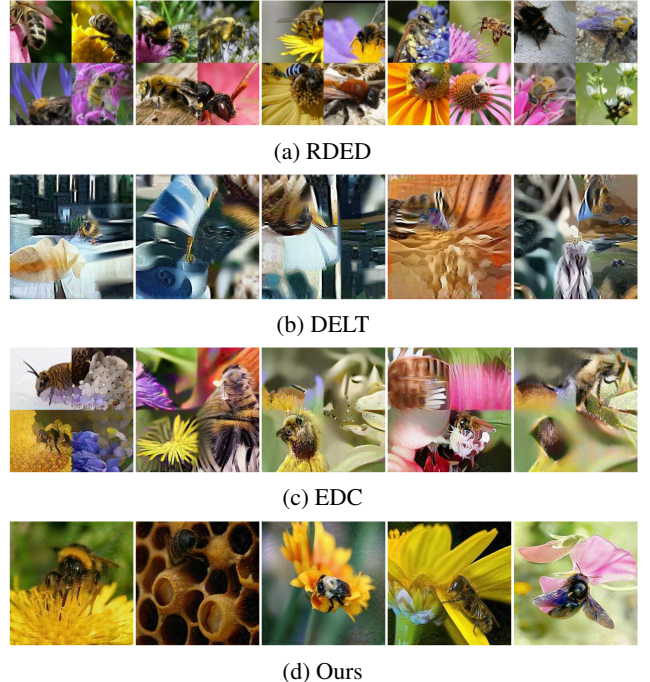


Figure 3. Visual comparison of synthetic data generated by SRe<sup>2</sup>L, RDED, DELLT, EDC, and our method E<sup>2</sup>D, which produces more diverse, less redundant samples and preserves semantic integrity with full-size feature representations.

## 3. Methodology

### 3.1. Preliminaries

Let  $\mathcal{D} = \{(x_i, y_i)\}_{i=1}^N$  be the original training dataset, where  $x_i \in \mathbb{R}^{H \times W \times C}$  is an image, and  $y_i \in \{1, \dots, L\}$  is its ground-truth label. Dataset distillation aims to synthesize a compact dataset  $\mathcal{S} = \{(\tilde{x}_j, \tilde{y}_j)\}_{j=1}^M$  with  $M \ll N$ , such that a model trained on  $\mathcal{S}$  achieves competitive performance compared to training on  $\mathcal{D}$ , by effectively capturing essential and diverse information within  $\mathcal{D}$ .

### 3.2. Overview

We study efficiency bottlenecks in recent decoupled dataset distillation methods and identify redundancy in two aspects of the pipeline: (i) suboptimal initialization that burdens the optimization with unnecessary corrective updates, and (ii) prolonged optimization that increasingly reinforces redundant signals and constrains efficiency. While prior work has primarily focused on improving diversity through architectural choices or data sampling strategies, we observe that excessive optimization signals not only increase synthesis cost but can also degrade instance-level feature richness, leading to negative returns. Our analysis shows that full-image initialization provides a substantially stronger starting point than the patch-based schemes commonly used in prior work [5, 25, 26, 29, 32]. Building on these insights, we propose a novel optimization strategy that mitigates re-

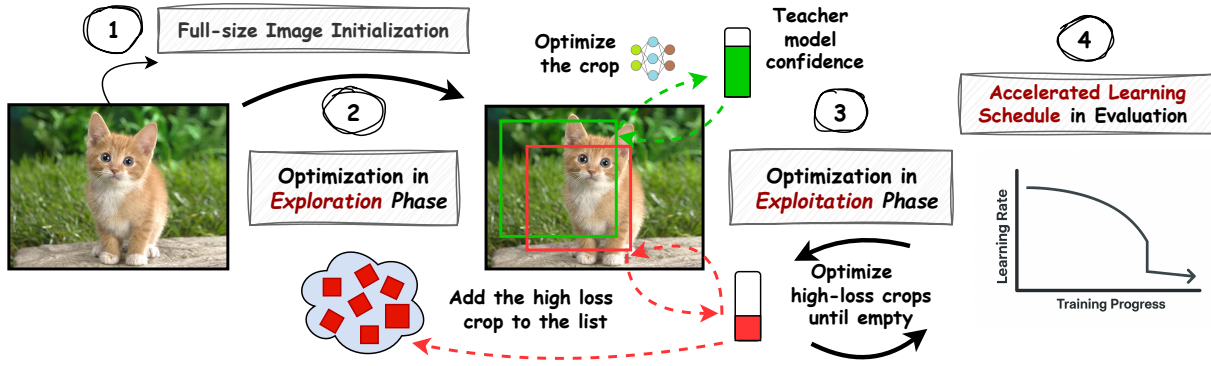


Figure 4. Overview of our proposed method E<sup>2</sup>D. The pipeline consists of four components: (1) **Full-size Image Initialization**, which preserves the semantic and structural information of the original data, preventing distortion or redundancy; (2) **Exploration Phase**, which identifies challenging high-loss regions and ensure balanced optimization; (3) **Exploitation Phase**, which iteratively refines these challenging regions for efficient convergence; and (4) **Accelerated Learning Schedule**, applied during student training to further speed up convergence. Together, these components enable fast and effective dataset distillation with minimal redundancy.

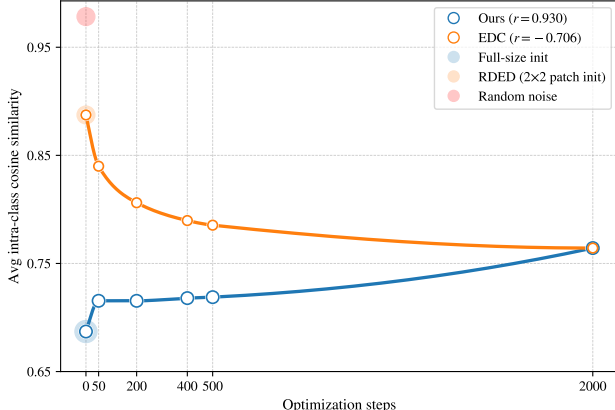


Figure 5. Cosine similarity trends across optimization steps.

dundancy, preserves diversity and accelerate convergence.

### 3.3. Redundancy in Initialization and Optimization

We treat redundancy as the degree of similarity between synthetic instances, viewing it as the opposite of diversity. Since diversity is inherently multi-dimensional, we adopt a practical proxy based on pairwise cosine similarity of teacher features. Higher similarity indicates more redundant representations, whereas lower similarity reflects greater instance-level diversity. Using this measure, we examine how teacher feature representations evolve under patch-based and full-image initialization, and how subsequent optimization amplifies or reduces redundant signals.

As shown in Fig. 5, patch-based initialization exhibits high redundancy and distorted feature representations, behaving closer to random noise than to the original data distribution captured by full-image initialization. In this regime, global-statistics optimization acts as a corrective step, reduc-

ing redundancy by steering noisy and misaligned features toward meaningful class-level structure. In contrast, when optimization is applied to full-image initialization, where features already align with the data distribution, the same global objective behaves differently. Rather than correcting noise, continued global alignment progressively amplifies shared class-level signals, increasing redundancy and eroding instance-level diversity over time. This reveals a conditional behavior of global-statistics optimization: it is beneficial when representations are far from the target distribution, but increasingly redundant once coarse alignment has been achieved.

Motivated by these observations, we aim to accelerate synthesis by controlling redundancy during optimization while retaining strong class-level supervision. Rather than adding new objectives, we control when global updates are applied by allowing broad corrective optimization early and then limiting redundant updates once representations are aligned. This preserves instance-level diversity inherited from full-image initialization while improving synthesis efficiency.

### 3.4. Exploration–Exploitation Optimization Strategy

We propose a two-phase optimization strategy that mitigates the redundancy of random multi-crop updates used in prior methods [7, 25, 37]. In conventional multi-crop optimization, each iteration performs in-place updates on randomly sampled local regions, repeatedly visiting similar patches and generating redundant learning signals. Inspired by the *exploration–exploitation* trade-off in reinforcement learning [11], our method separates this process into distinct exploration–exploitation phases to achieve efficient coverage

---

**Algorithm 1:** Exploration–Exploitation Distillation (E<sup>2</sup>D)

---

**Input:** Original dataset  $\mathcal{D}$ , teacher model  $\mathcal{T}$ , loss threshold  $\epsilon$ , exploration iterations  $K$ , total iterations  $T$

**Output:** Updated synthetic dataset  $\mathcal{S}$

```

1 foreach  $(x_i, y_i) \sim \mathcal{S}$  do
2   /* Exploration Phase */ *
3   Initialize  $\mathcal{M}_i \leftarrow \emptyset$ 
4   Initialize  $x_i$  with a random image from  $\mathcal{D}$ 
5   for  $t = 1$  to  $K$  do
6      $\tilde{x}_i \leftarrow \text{RandomResizedCrop}(x_i)$ 
7      $l_i = \mathcal{L}_{ce}(\mathcal{T}(\tilde{x}_i), y_i)$ ;
8     if  $l_i > \epsilon$  then
9       Store (crop coordinates,  $l_i$ ) in  $\mathcal{M}_i$ ;
10    Update  $\tilde{x}_i$  using the baseline distillation loss.
11  /* Exploitation Phase */ *
12  for  $t = K + 1$  to  $T$  do
13    if  $\mathcal{M}_i \neq \emptyset$  then
14      Sample (crop coordinates) from  $\mathcal{M}_i$  via
15      softmax over  $l_i$ ;
16       $\tilde{x}_i \leftarrow \text{Crop}(x_i, \text{crop coordinates})$ ;
17       $l'_i = \mathcal{L}_{ce}(\mathcal{T}(\tilde{x}_i), y_i)$ ;
18      if  $l'_i > \epsilon$  then
19        Update stored loss in  $\mathcal{M}_i$ ;
20      else
21        Remove crop from  $\mathcal{M}_i$ ;
22      else
23        /* Early Stopping */ *
24        break
25    Update  $\tilde{x}_i$  using the baseline distillation loss.

```

---

and targeted refinement, directing computation toward regions with strong learning potential to increase information density and accelerate convergence. Our method is formally outlined in Algorithm 1.

**Exploration Phase.** This phase performs random multi-crop optimization over  $K$  iterations to broadly update the synthetic data and record informative regions. For each synthetic image  $x_i$ , crops that yield high teacher loss  $\mathcal{L}_{ce}(\mathcal{T}(\tilde{x}_i), y_i) > \epsilon$  are stored with their coordinates and loss values in a per-image memory buffer  $M_i$ . These buffers accumulate the teacher’s uncertainty landscape, identifying regions that are under-optimized or poorly aligned with class semantics. The same random crop is applied to all images in the batch to maintain computational efficiency.

**Exploitation Phase.** After  $K$  exploration iterations, optimization shifts to focused refinement of the high-loss regions identified in the exploration phase. For each synthetic image  $x_i$ , crops are sampled from its buffer  $M_i$  with probabilities

proportional to their stored losses:

$$p_{ij} = \frac{\exp(\ell_{ij})}{\sum_{k=1}^{N_i} \exp(\ell_{ik})} \quad (1)$$

where  $p_{ij}$  denotes the probability of selecting the  $j$ -th high-loss crop in image  $x_i$ ,  $\ell_{ij}$  represents the loss of the  $j$ -th crop in image  $x_i$ , and  $N_i$  indicates the total number of crops stored in the buffer  $M_i$ .

This softmax weighting prioritizes difficult regions while maintaining diversity among selected crops. Updated losses are re-evaluated and refreshed in memory; regions that fall below the loss threshold are discarded, preventing redundant computation on well-optimized areas.

Optimization proceeds until all buffers are emptied or the maximum iteration budget  $T$  is reached. Early stopping prevents over-optimization of the distilled data, preserving image features inherited from the original dataset.

## 4. Experiments

To evaluate our method, we perform experiments on two large-scale datasets using multiple model architectures to assess its effectiveness and its ability to generalize across architectures. We conduct comprehensive ablations and convergence analyses, examining how varying acceleration factors, including optimization-free settings affect the efficiency–performance trade-off.

### 4.1. Experimental Setups

**Datasets.** We evaluate our method on two large-scale and computationally intensive benchmarks: ImageNet-1K [6] and ImageNet-21K-P (referred to as ImageNet-21K throughout the paper) [22]. ImageNet-1K consists of 1,000 classes and 1.28 million images, while ImageNet-21K includes 10,450 classes and over 11 million images. We omit results on small-scale datasets (e.g., CIFAR-10/100), where our baseline EDC already achieves state-of-the-art performance with very few optimization iterations, which makes further acceleration provide negligible efficiency gains. Additional discussion is provided in the appendix.

**Network architectures.** For Tab. 1 and Tab. 2, we report results using the widely adopted ResNet-18 architecture as the evaluation model. Following previous works [25, 36], and to ensure the distilled data are not overfitted to any single architecture, we further assess cross-architecture generalization on diverse models including ResNet-{50,101} [9], MobileNet-V2 [23], EfficientNet-B0 [30], ConvNext-Tiny [16], ShuffleNet-V2 [18], DeiT-Tiny [31], RegNet-Y-8GF [21], and DenseNet-121 [10].

**Baselines.** We compare against recent state-of-the-art methods in large-scale dataset distillation. For ImageNet-1K, we compare with SRe<sup>2</sup>L [37], CDA [36], DWA [7], G-VBSM [24], RDED [29], DELT [26], and EDC [25]. On

Dataset	IPC	ResNet-18						
		SRe <sup>2</sup> L	CDA	DWA	RDED	DELT	Ours <sub>(optimization-free)</sub>	Ours <sub>10×</sub>
ImageNet-1K	1	–	–	–	6.6 ± 0.2	–	12.8 ± 0.1	11.5 ± 0.4
	10	21.3 ± 0.6	31.4 ± 0.5	33.5 ± 0.3	37.9 ± 0.2	46.1 ± 0.4	48.6 ± 0.3	50.0 ± 0.1
	50	46.8 ± 0.2	51.8 ± 0.4	53.5 ± 0.3	55.2 ± 0.2	<b>59.2 ± 0.4</b>	58.0 ± 0.2	58.9 ± 0.1

Table 1. **Comparison of dataset distillation methods on ImageNet-1K using ResNet-18 as the evaluation model.** Our method is presented in two variants: with an acceleration factor of  $10\times$  and an optimization-free variant. Our results are reported as mean  $\pm$  standard deviation over five evaluation models, each randomly initialized and trained independently on the distilled dataset. Missing entries (–) indicate results not reported in the original work.

Dataset	IPC	ResNet-18				
		SRe <sup>2</sup> L	CDA	D3S	Ours <sub>(optimization-free)</sub>	Ours <sub>5×</sub>
ImageNet-21K	10	18.5 ± 0.2	22.6 ± 0.2	26.9 ± 0.1	28.8 ± 0.02	<b>32.1 ± 0.4</b>
	20	21.8 ± 0.1	26.4 ± 0.1	28.5 ± 0.1	33.9 ± 0.1	<b>36.0 ± 0.1</b>

Table 2. **Comparison of dataset distillation methods on ImageNet-21K using ResNet-18 as the evaluation model.** Our method is presented with an acceleration factor of  $5\times$ , along with an optimization-free variant. Our results are reported as mean  $\pm$  standard deviation over three evaluation models, each randomly initialized and trained independently on the distilled dataset.

ImageNet-21K, we consider SRe<sup>2</sup>L, CDA, and D3S [17] as baselines.

**Implementation details.** We adopt EDC as the implementation backbone for our method in ImageNet-1K and CDA in ImageNet-21K. Both are accelerated using our Exploration–Exploitation strategy, allocating 70% of iterations to exploration and the remaining 30% to exploitation. Our method integrates seamlessly with state-of-the-art methods, demonstrating its adaptability cross both large-scale datasets and different distillation methods. EDC and CDA are optimized for 2000 iterations, and our reported acceleration factors are measured relative to this budget. When extending our method to ImageNet-21K, we reused the optimization hyperparameters from prior work. Under this setup, even slight optimization caused performance to degrade below that of the optimization-free variant. We attribute this to a distributional mismatch between the teacher model and the synthesized data. To mitigate this, we reduced the learning rate and relaxed the batch-normalization regularization term  $\alpha_{BN}$ , which stabilized optimization and yielded smoother convergence curves. Additional implementation details and hyperparameter configurations are provided in the appendix.

## 4.2. Results

Our method demonstrates strong performance as shown in Tab. 1 and Tab. 2. Despite being several folds more efficient, it consistently achieves superior accuracy compared to recent state-of-the-art methods.

On ImageNet-1K, our method sets a new benchmark at the highly compressed  $IPC = 10$  setting, reaching 50% accuracy. On the more challenging ImageNet-21K, it delivers a substantial improvement by achieving 32.1% accuracy at  $IPC = 10$ . While the performance gap narrows

as  $IPC$  increases, our method continues to outperform state-of-the-art methods, achieving 58.9% on ImageNet-1K at  $IPC = 50$  and 36% on ImageNet-21K at  $IPC = 20$ . Our optimization-free variant performs on par with the strongest prior method, EDC, on ImageNet-1K, despite requiring no optimization. Remarkably, on ImageNet-21K, our optimization-free variant outperforms all existing methods while using only half the distillation budget ( $IPC = 10$ ) compared to state-of-the-art methods trained at  $IPC = 20$ .

## 4.3. Cross-architecture Generalization

A key property of distilled datasets is their ability to generalize across diverse model architectures. We evaluate our method against its closest baselines on a range of architectures, as shown in Tab. 3 for ImageNet-1K and Tab. 4 for ImageNet-21K. Our method consistently outperforms state-of-the-art methods across all models, demonstrating improved robustness and consistently superior cross-architecture performance.

## 4.4. Acceleration and Efficiency

**Acceleration of Optimization.** We study how accelerating our method influences performance relative to the EDC baseline on ImageNet-1K. As shown in Fig. 6, optimization-free settings generally perform increasingly close to the optimization-based ones as the  $IPC$  increases, a trend also observed in prior work [35]. Notably, our method in the optimization-free setting nearly matches the performance of the optimized version at high  $IPC$ , highlighting its efficiency given the substantial cost of optimization at large  $IPC$ . The  $20\times$  accelerated variant of our method results in less than 0.1% accuracy drop, striking an effective balance between speed and performance. The  $10\times$  accelerated version of

IPC	Method	Evaluation model						
		ResNet-18	ResNet-50	ResNet-101	MobileNet-V2	EfficientNet-B0	ConvNext-Tiny	ShuffleNet-V2
10	RDED	42.0	46.0	48.3	34.4	42.8	48.3	19.4
	EDC	48.6	54.1	51.7	45.0	51.1	54.4	29.8
	Ours <sub>10×</sub>	<b>50.0</b>	<b>55.6</b>	<b>54.7</b>	<b>46.9</b>	<b>52.9</b>	<b>55.0</b>	<b>45.4</b>
50	RDED	56.6	63.7	61.2	53.9	57.6	65.4	30.9
	EDC	58.0	64.3	64.9	57.8	60.9	66.6	45.7
	Ours <sub>10×</sub>	<b>58.9</b>	<b>64.7</b>	<b>65.1</b>	<b>58.1</b>	<b>61.3</b>	<b>66.8</b>	<b>56.4</b>

Table 3. Cross-architecture generalization performance on ImageNet-1K at IPC 10 and 50 across multiple evaluation models.

IPC	Method	Evaluation model					
		ResNet-18	ResNet-50	ResNet-101	DenseNet-121	RegNet-Y-8GF	ConvNeXt-Tiny
20	SRe <sup>2</sup> L	21.8	31.2	33.2	24.6	34.2	34.9
	CDA	26.4	35.3	36.1	28.6	36.1	36.3
	D3S	28.5	35.4	36.0	31.9	36.4	–
	Ours <sub>5×</sub>	<b>36.0</b>	<b>36.9</b>	<b>37.3</b>	<b>33.1</b>	<b>37.4</b>	<b>37.2</b>

Table 4. Cross-architecture generalization performance on ImageNet-21K data at IPC 20 across multiple evaluation models. Missing entries (–) indicate unreported results with no publicly available codebase.

our method is sufficient to reach convergence, while the 5× version does not provide additional gains. As the number of optimization steps approaches the standard 2000 iterations, both our method and the baseline converge in performance, suggesting that excessive optimization reinforces redundant signals and reduces instance-level diversity, supporting a counter-traditional view that more optimization is not necessarily better.

	Ours <sub>20×</sub>	Ours <sub>10×</sub>	EDC
Synthesis Time (hrs)	12.3	24.0	229.8
Synthesis Speedup	18.6×	9.5×	1.0×

(a) ImageNet-1K (IPC = 50)

	Ours <sub>10×</sub>	Ours <sub>5×</sub>	CDA
Synthesis Time (hrs)	38.8	67.7	296.5
Synthesis Speedup	7.6×	4.3×	1.0×

(b) ImageNet-21K (IPC = 20)

Table 5. **Synthesis time and acceleration factor comparison.** Each subtable reports synthesis time (hours) and speedup over baseline on a single NVIDIA RTX A6000 GPU with ResNet-18, evaluated on different datasets.

**Efficiency Comparison.** We compute the actual acceleration factor of our method, accounting for the overhead introduced by the Exploration–Exploitation strategy. To ensure fair comparison, all experiments are conducted on a single NVIDIA RTX A6000 GPU, and synthesis time is reported excluding data and model loading overhead.

As shown in Tab. 5, our method accelerates EDC by over

**18×** while maintaining higher near-converged accuracy. The additional cost of the Exploration–Exploitation optimization strategy remains modest relative to the **2×** improvement in synthesis efficiency (see Tab. 6 in the study). Beyond synthesis speed, we also address memory efficiency by applying Automatic Mixed Precision (AMP) to the forward pass of the bottleneck backbone architecture, EfficientNet-B0. This tweak reduces peak GPU memory consumption from 16.05 GB to 14 GB without any measurable loss in accuracy, allowing our method to fit comfortably on a single 16 GB GPU.

For ImageNet-21K, our method also improves CDA efficiency, though the gain is smaller due to the dataset’s large-scale, which increases the cost of maintaining high-loss crop buffers compared to random cropping. Nevertheless, our method achieves consistently faster synthesis with stronger accuracy across both benchmarks.

## 4.5. Discussion

### Effectiveness of Exploration–Exploitation Strategy

We evaluate the impact of our Exploration–Exploitation strategy against the random multi-crop optimization used in the baselines. As shown in Tab. 6, our method outperforms the baseline even when the latter is given twice the optimization budget, enabling up to 2× faster convergence during synthesis.

### Design Space of E<sup>2</sup>D.

To examine the design space of our exploration–exploitation method, we evaluate four variants in Tab. 7. **(1) Exploit only.** Image updates occur exclusively during exploitation, while exploration evaluates random crops using the teacher loss without performing any

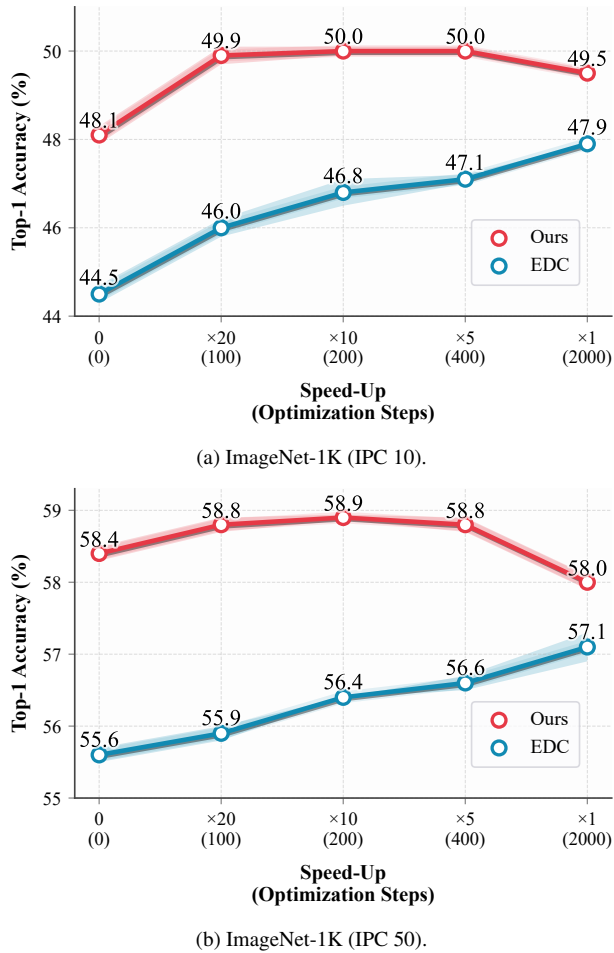


Figure 6. Top-1 accuracy vs. speedup for our method and baseline EDC under two IPC settings. Our method converges faster and starts from a stronger no-optimization starting point. In our method, extra optimization past convergence degrades performance, counter to the common assumption that more optimization is always better.

IPC	Ours <sub>20×</sub> (R)	Ours <sub>20×</sub> (E <sup>2</sup> )	Ours <sub>10×</sub> (R)
10	$49.7 \pm 0.2$	<b><math>49.9 \pm 0.1</math></b>	$49.8 \pm 0.1$
50	$58.4 \pm 0.1$	<b><math>58.8 \pm 0.04</math></b>	$58.8 \pm 0.1$

Table 6. **Effectiveness of Exploration–Exploitation strategy.** Ablation of our Exploration–Exploitation optimization (E<sup>2</sup>) vs. random multi-crop optimization (R) on ImageNet-1K. E<sup>2</sup> improves accuracy and enables up to 2× faster convergence during synthesis.

image-level updates. **(2) GradCAM-guided probing.** For each synthetic image, a GradCAM map is computed, and crops are sampled inversely to the activation magnitude so that low-activation regions are prioritized. **(3) Alternating cycles.** A periodic schedule of twenty steps in which exploration and exploitation alternate, replacing our two-stage procedure. **(4) Random multi-crop optimization.** The default strategy adopted in prior work, where crops

are sampled uniformly at random throughout optimization. Across these variants, our method achieves the strongest performance. The drop in the exploit-only setting highlights the importance of uniform image-level updates, and the GradCAM variant further shows that semantic activation maps alone are insufficient, performing worse than simple random cropping.

IPC	Exploit-Only	Grad-CAM	Alt. Cycles	Random Crop	E <sup>2</sup> D
10	$48.5 \pm 0.2$	$49.4 \pm 0.2$	$49.6 \pm 0.2$	$49.7 \pm 0.2$	<b><math>49.9 \pm 0.1</math></b>

Table 7. Ablation of the design space of E<sup>2</sup>D under a  $\times 20$  acceleration factor on ImageNet-1K (IPC 10).

### When to Switch to Exploitation Phase

We analyze the effect of switching from exploration to exploitation at different points, controlled by hyperparameter  $K$ . If  $K$  is too small, the switch is premature and crop diversity suffers; if too large, it degenerates to random cropping. Our experiments show that performance remains stable across a broad range of  $K$  values, suggesting robustness to the exact choice of  $K$ . As shown in Tab. 8, allocating 70% of the iterations to exploration and 30% to exploitation yields the best accuracy, offering an effective balance between crop diversity and targeted refinement.

K	40	60	70	80
Ours <sub>20×</sub>	$49.7 \pm 0.2$	$49.8 \pm 0.1$	<b><math>49.9 \pm 0.1</math></b>	$49.7 \pm 0.1$

Table 8. **When to switch to exploitation.** Ablation study on the number of exploration iterations  $K$  (out of 100 total iterations) for our method accelerated by 20× on ImageNet-1K with IPC = 10.

## 5. Conclusion

We introduced Exploration–Exploitation Distillation (E<sup>2</sup>D), a redundancy-reducing method for efficient large-scale dataset distillation. E<sup>2</sup>D integrates full-image initialization, targeted Exploration–Exploitation optimization, and an accelerated student schedule to minimize redundant updates while preserving diversity. Evaluated on two large-scale benchmarks, ImageNet-1K and ImageNet-21K, E<sup>2</sup>D achieves higher accuracy with substantially lower synthesis cost. These findings show that greater accuracy does not require more optimization; rather, directing computation where it matters most leads to better accuracy–efficiency trade-offs in large-scale dataset distillation.

**Limitations and Future Work.** Our method does not account for the cost/efficiency of the relabeling stage or of constructing or selecting the pretrained models and collecting their statistics. We rely on simple random sampling for initialization, but more robust strategies may lead to more consistent performance. Furthermore, bridging the accuracy–efficiency gap at higher IPC levels may require refined optimization and initialization strategies beyond existing approaches.

## Acknowledgments

This work was partially supported by the National Science Foundation (NSF) grants BCS-2416846, OAC-2417850, and DUE-2526340. Muhammad J. Alahmadi is supported in part by King Abdulaziz University (KAU). This research used resources of the Oak Ridge Leadership Computing Facility at Oak Ridge National Laboratory, supported by the Office of Science of the U.S. Department of Energy under Contract No. DE-AC05-00OR22725. The views and conclusions are those of the authors and should not be interpreted as representing the official policies of the funding agencies or the government.

## References

- [1] Ondrej Bohdal, Yongxin Yang, and Timothy Hospedales. Flexible dataset distillation: Learn labels instead of images. *arXiv preprint arXiv:2006.08572*, 2020. 1
- [2] George Cazenavette, Tongzhou Wang, Antonio Torralba, Alexei A. Efros, and Jun-Yan Zhu. Wearable imangenet: Synthesizing tileable textures via dataset distillation. In *Proceedings of the IEEE/CVF Conference on Computer Vision and Pattern Recognition Workshops (CVPRW)*, 2022. 1, 3
- [3] George Cazenavette, Tongzhou Wang, Antonio Torralba, Alexei A. Efros, and Jun-Yan Zhu. Generalizing dataset distillation via deep generative prior. *Proceedings of the IEEE/CVF Conference on Computer Vision and Pattern Recognition (CVPR)*, 2023. 3
- [4] Justin Cui, Ruochen Wang, Si Si, and Cho-Jui Hsieh. Scaling up dataset distillation to imagenet-1k with constant memory. In *International Conference on Machine Learning (ICML)*, pages 6565–6590. PMLR, 2023. 3
- [5] Jiacheng Cui, Zhaoyi Li, Xiaochen Ma, Xinyue Bi, Yixin Luo, and Zhiqiang Shen. Dataset distillation via committee voting, 2025. 3, 1
- [6] Jia Deng, Wei Dong, Richard Socher, Li-Jia Li, Kai Li, and Li Fei-Fei. Imagenet: A large-scale hierarchical image database. In *2009 IEEE Conference on Computer Vision and Pattern Recognition (CVPR)*, pages 248–255, 2009. 5
- [7] Jiawei Du, Xin Zhang, Juncheng Hu, Wenxin Huang, and Joey Tianyi Zhou. Diversity-driven synthesis: Enhancing dataset distillation through directed weight adjustment. In *Advances in Neural Information Processing Systems (NeurIPS)*, 2024. 2, 3, 4, 5, 1
- [8] Jianyang Gu, Saeed Vahidian, Vyacheslav Kungurtsev, Haonan Wang, Wei Jiang, Yang You, and Yiran Chen. Efficient dataset distillation via minimax diffusion. In *Proceedings of the IEEE/CVF Conference on Computer Vision and Pattern Recognition (CVPR)*, 2024. 3
- [9] Kaiming He, Xiangyu Zhang, Shaoqing Ren, and Jian Sun. Deep residual learning for image recognition. In *2016 IEEE Conference on Computer Vision and Pattern Recognition (CVPR)*, pages 770–778, 2016. 5
- [10] Gao Huang, Zhuang Liu, Laurens Van Der Maaten, and Kilian Q. Weinberger. Densely connected convolutional networks. In *2017 IEEE Conference on Computer Vision and Pattern Recognition (CVPR)*, pages 2261–2269, 2017. 5
- [11] Leslie Pack Kaelbling, Michael L Littman, and Andrew W Moore. Reinforcement learning: A survey. *Journal of Artificial Intelligence Research*, 4:237–285, 1996. 4
- [12] Jang-Hyun Kim, Jinuk Kim, Seong Joon Oh, Sangdoo Yun, Hwanjun Song, Joonhyun Jeong, Jung-Woo Ha, and Hyun Oh Song. Dataset condensation via efficient synthetic-data parameterization. In *International Conference on Machine Learning (ICML)*, 2022. 1, 3
- [13] Guang Li, Bo Zhao, and Tongzhou Wang. Awesome dataset distillation github repo, 2022. 3
- [14] Hongcheng Li, Yucan Zhou, Xiaoyan Gu, Bo Li, and Weiping Wang. Diversified semantic distribution matching for dataset distillation. In *Proceedings of the 32nd ACM International Conference on Multimedia*, page 7542–7550, New York, NY, USA, 2024. Association for Computing Machinery. 3
- [15] Yanqing Liu, Jianyang Gu, Kai Wang, Zheng Zhu, Wei Jiang, and Yang You. DREAM: Efficient dataset distillation by representative matching. *arXiv preprint arXiv:2302.14416*, 2023. 3
- [16] Zhuang Liu, Hanzi Mao, Chao-Yuan Wu, Christoph Feichtenhofer, Trevor Darrell, and Saining Xie. A convnet for the 2020s. In *Proceedings of the IEEE/CVF Conference on Computer Vision and Pattern Recognition (CVPR)*, 2022. 5
- [17] Noel Loo, Alaa Maalouf, Ramin Hasani, Matthias Lechner, Alexander Amini, and Daniel Rus. Large scale dataset distillation with domain shift. In *Proceedings of the 41st International Conference on Machine Learning (ICML)*. JMLR.org, 2024. 6
- [18] Ningning Ma, Xiangyu Zhang, Hai-Tao Zheng, and Jian Sun. Shufflenet v2: Practical guidelines for efficient cnn architecture design. In *Proceedings of the European Conference on Computer Vision (ECCV)*, 2018. 5
- [19] Ding Qi, Jian Li, Junyao Gao, Shuguang Dou, Ying Tai, Jianlong Hu, Bo Zhao, Yabiao Wang, Chengjie Wang, and Cairong Zhao. Towards universal dataset distillation via task-driven diffusion. In *Proceedings of the IEEE/CVF Conference on Computer Vision and Pattern Recognition (CVPR)*, pages 10557–10566, 2025. 3
- [20] Tian Qin, Zhiwei Deng, and David Alvarez-Melis. A label is worth a thousand images in dataset distillation. In *Advances in Neural Information Processing Systems (NeurIPS)*, pages 131946–131971. Curran Associates, Inc., 2024. 1
- [21] Ilija Radosavovic, Raj Prateek Kosaraju, Ross Girshick, Kaiming He, and Piotr Dollar. Designing network design spaces. In *Proceedings of the IEEE/CVF Conference on Computer Vision and Pattern Recognition (CVPR)*, 2020. 5
- [22] Tal Ridnik, Emanuel Ben Baruch, Asaf Noy, and Lihi Zelnik-Manor. Imagenet-21k pretraining for the masses. *CoRR*, abs/2104.10972, 2021. 5
- [23] Mark Sandler, Andrew Howard, Menglong Zhu, Andrey Zhmoginov, and Liang-Chieh Chen. MobileNetV2: Inverted Residuals and Linear Bottlenecks. In *2018 IEEE/CVF Conference on Computer Vision and Pattern Recognition (CVPR)*, pages 4510–4520, Los Alamitos, CA, USA, 2018. IEEE Computer Society. 5
- [24] Shitong Shao, Zeyuan Yin, Muxin Zhou, Xindong Zhang, and Zhiqiang Shen. Generalized large-scale data condensation via

various backbone and statistical matching. In *Proceedings of the IEEE/CVF Conference on Computer Vision and Pattern Recognition (CVPR)*, pages 16709–16718, 2024. 2, 3, 5

[25] Shitong Shao, Zikai Zhou, Huanran Chen, and Zhiqiang Shen. Elucidating the design space of dataset condensation. In *Advances in Neural Information Processing Systems (NeurIPS)*, pages 99161–99201. Curran Associates, Inc., 2024. 1, 2, 3, 4, 5

[26] Zhiqiang Shen, Ammar Sherif, Zeyuan Yin, and Shitong Shao. Delt: A simple diversity-driven earlylate training for dataset distillation. In *Proceedings of the IEEE/CVF Conference on Computer Vision and Pattern Recognition (CVPR)*, 2025. 2, 3, 5, 1

[27] Rui Song, Dai Liu, Dave Zhenyu Chen, Andreas Festag, Carsten Trinitis, Martin Schulz, and Alois Knoll. Federated learning via decentralized dataset distillation in resource-constrained edge environments. *arXiv preprint arXiv:2208.11311*, 2022. 1

[28] Duo Su, Junjie Hou, Weizhi Gao, Yingjie Tian, and Bowen Tang. D^4: Dataset distillation via disentangled diffusion model. In *Proceedings of the IEEE/CVF Conference on Computer Vision and Pattern Recognition (CVPR)*, pages 5809–5818, 2024. 3

[29] Peng Sun, Bei Shi, Daiwei Yu, and Tao Lin. On the diversity and realism of distilled dataset: An efficient dataset distillation paradigm. In *Proceedings of the IEEE/CVF Conference on Computer Vision and Pattern Recognition (CVPR)*, 2024. 1, 2, 3, 5

[30] Mingxing Tan and Quoc V. Le. Efficientnet: Rethinking model scaling for convolutional neural networks. *CoRR*, abs/1905.11946, 2019. 5

[31] Hugo Touvron, Matthieu Cord, Matthijs Douze, Francisco Massa, Alexandre Sablayrolles, and Herve Jegou. Training data-efficient image transformers and distillation through attention. In *Proceedings of the 38th International Conference on Machine Learning (ICML)*, pages 10347–10357. PMLR, 2021. 5

[32] Minh-Tuan Tran, Trung Le, Xuan-May Le, Thanh-Toan Do, and Dinh Phung. Enhancing dataset distillation via non-critical region refinement. In *2025 IEEE/CVF Conference on Computer Vision and Pattern Recognition (CVPR)*, pages 10015–10024, 2025. 1, 3

[33] Kai Wang, Bo Zhao, Xiangyu Peng, Zheng Zhu, Shuo Yang, Shuo Wang, Guan Huang, Hakan Bilen, Xinchao Wang, and Yang You. Cafe: Learning to condense dataset by aligning features. In *Proceedings of the IEEE/CVF Conference on Computer Vision and Pattern Recognition (CVPR)*, pages 12196–12205, 2022. 1, 3

[34] Tongzhou Wang, Jun-Yan Zhu, Antonio Torralba, and Alexei A Efros. Dataset distillation. *arXiv preprint arXiv:1811.10959*, 2018. 1

[35] Lingao Xiao, Songhua Liu, Yang He, and Xinchao Wang. Rethinking large-scale dataset compression: Shifting focus from labels to images. *arXiv preprint arXiv:2502.06434*, 2025. 1, 6

[36] Zeyuan Yin and Zhiqiang Shen. Dataset distillation via curriculum data synthesis in large data era. *Transactions on Machine Learning Research*, 2024. 3, 5

[37] Zeyuan Yin, Eric Xing, and Zhiqiang Shen. Squeeze, recover and relabel: Dataset condensation at imagenet scale from a new perspective. In *Advances in Neural Information Processing Systems (NeurIPS)*, 2023. 1, 2, 3, 4, 5

[38] Lei Zhang, Jie Zhang, Bowen Lei, Subhabrata Mukherjee, Xiang Pan, Bo Zhao, Caiwen Ding, Yao Li, and Dongkuan Xu. Accelerating dataset distillation via model augmentation. In *2023 IEEE/CVF Conference on Computer Vision and Pattern Recognition (CVPR)*, pages 11950–11959, 2023. 1, 3

[39] Bo Zhao and Hakan Bilen. Dataset condensation with differentiable siamese augmentation. In *International Conference on Machine Learning (ICML)*, 2021. 1, 3

[40] Bo Zhao and Hakan Bilen. Synthesizing informative training samples with gan. *NeurIPS 2022 Workshop on Synthetic Data for Empowering ML Research*, 2022. 3

[41] Bo Zhao and Hakan Bilen. Dataset condensation with distribution matching. In *Proceedings of the IEEE/CVF Winter Conference on Applications of Computer Vision*, 2023. 3

[42] Bo Zhao, Konda Reddy Mopuri, and Hakan Bilen. Dataset condensation with gradient matching. In *International Conference on Learning Representations*, 2021. 1, 3

[43] Xinhao Zhong, Hao Fang, Bin Chen, Xulin Gu, Tao Dai, Meikang Qiu, and Shu-Tao Xia. Hierarchical features matter: A deep exploration of gan priors for improved dataset distillation. *arXiv preprint arXiv:2406.05704*, 2024. 3

[44] Xinhao Zhong, Shuoyang Sun, Xulin Gu, Zhaoyang Xu, Yaowei Wang, Min Zhang, and Bin Chen. Efficient dataset distillation via diffusion-driven patch selection for improved generalization, 2025. 2, 3

[45] Yongchao Zhou, Ehsan Nezhadarya, and Jimmy Ba. Dataset distillation using neural feature regression. In *Advances in Neural Information Processing Systems (NeurIPS)*, 2022. 3

# Accelerating Large-Scale Dataset Distillation via Exploration–Exploitation Optimization

## Supplementary Material

### 6. Further Discussion

#### Additional Cross-architecture Evaluation.

To expand our evaluation of cross-architecture generalization, Tab. 11 reports results on transformer-based and hybrid models, where our method consistently achieves the strongest performance.

**Full-size Image Initialization** We adopt real image initialization sampled from the original dataset, which accelerates distillation compared to random noise, as observed in prior works [5, 7, 25, 26, 38]. Our closest baseline, EDC, relies on RDED [29] for fast, optimization-free initialization by composing each synthetic image from several high-confidence patches of real data. However, patch-based compression oversamples similar regions, which leads to redundancy, and it further distorts local features because of the compressed representation. We further posit that the subsequent relabeling stage, which functions as knowledge distillation, may be less effective under patch-based representations, as fragmented local regions provide limited global context for transferring semantic knowledge from teacher to student. In contrast, full-image initialization preserves global semantics and spatial coherence, improving generalization and convergence while simplifying deployment by removing the pre-synthesis step. At  $IPC = 1$ , we adopt RDED for its stronger performance under extreme data scarcity, but we downplay this case because single-image settings yield unstable accuracy across runs.

#### Initialization Sensitivity in Extremely Compressed IPC

Table 13 reports three runs of our method at  $IPC = 1$  with different RDED initialization seeds. Performance varies by up to 2%, highlighting the instability caused by different initializations and the challenge of fair comparison in such an extreme compression setting.

#### Full-size vs. Patch-Based Initialization

We compare our full-size image initialization with EDC’s patch-based initialization. For  $IPC = 10$ , EDC initializes each synthetic image using RDED with four crops per image setting, while our method directly samples full-size images. For  $IPC = 50$ , to test an alternative setup and further validate our method’s effectiveness, we set EDC to be initialized from a single crop per image, a setting that empirically yields better accuracy, with SSRS learning schedule applied to both methods. All results are reported without the optimization stage to isolate the effect of initialization. As shown in Tab. 14, full-size initialization consistently yields higher accuracy than patch-based initialization, providing a stronger starting point that enables subsequent optimization to be

more efficient.

#### Relabeling and Post-Evaluation Strategies

For relabeling, we follow the standard state-of-the-art approach for generating soft labels from the teacher model. During student training on distilled data, we adopt the *Early Smoothing–Later Steep Learning Rate Schedule* (SSRS) introduced in EDC [25]. SSRS combines the advantages of smooth cosine decay and MultiStep schedules by applying a gradual cosine reduction in the early phase, followed by a sharp decay in the final phase to accelerate convergence as described in this equation:

$$\mu(i) = \begin{cases} \frac{1 + \cos\left(\frac{i\pi}{\zeta N}\right)}{2}, & i \leq \frac{5N}{6}, \\ \frac{1 + \cos\left(\frac{5\pi}{6\zeta}\right)}{2} \cdot \frac{6N - 6i}{6N}, & i > \frac{5N}{6}, \end{cases} \quad (2)$$

where  $\mu(i)$  is the learning rate at iteration  $i$ ,  $N$  is the total number of training iterations, and  $\zeta$  controls the cosine smoothness. Unlike EDC, which introduced SSRS only in the appendix and considered it in high-IPC settings, our method demonstrates that applying this schedule at moderate IPC also improves accuracy. Additionally, it reduces the synthesis time required to reach peak accuracy, highlighting a connection between student training dynamics and distillation efficiency.

#### Effectiveness of Early Smoothing–later Steep Learning Rate Schedule (SSRS)

To evaluate the effectiveness of SSRS, we compare our method with and without it under various IPC settings. While performance drops significantly at extremely low IPC values (e.g.,  $IPC = 1$ ), SSRS consistently improves results at higher IPCs by achieving better accuracy and requiring fewer optimization steps to reach convergence. As shown in Tab. 12, the benefits of SSRS become increasingly clear as IPC increases. Our method, accelerated 20 $\times$  with SSRS, achieves near-converged performance without additional computational cost. This observation is consistent with prior work [25], which shows that an effective learning schedule can yield substantial improvements with minimal overhead. Our findings further establish a connection between optimization efficiency and the design of the learning schedule, showing that accelerated learning scheduling can significantly reduce the need for extensive optimization.

#### Synthetic Data Comparison in Logit Space

Figure 7 presents t-SNE visualizations of logit embeddings for synthetic data generated by our method and recent state-

Synthesis		Relabeling & Evaluation	
Iteration	200	Epochs	300
Optimizer	AdamW	Optimizer	AdamW
	$\beta_1 = 0.5, \beta_2 = 0.9$		
Learning rate	0.05	Loss Type	MSE-GT + 0.025·CE
Batch Size	80	Learning rate	0.001
$K, \epsilon$	140, 0.5	Batch Size	100
Initialization	Random sampling (RDED at IPC = 1)	LR Schedule	SSRS, $\zeta = 2$ SmoothingLR at IPC = 1
$\alpha_{BN}$	0.1	Augmentation	RandomResizedCrop RandomHorizontalFlip CutMix
		EMA Rate	0.99

Table 9. Hyperparameter settings for ImageNet-1K.

Synthesis		Relabeling & Evaluation	
Iteration	400	Epochs	300
Optimizer	AdamW	Optimizer	AdamW
	$\beta_1 = 0.5, \beta_2 = 0.9$		
Learning rate	0.005	Loss Type	KL-Div
Batch Size	80	Learning rate	0.005
$K, \epsilon$	280, 0.3	Batch Size	100
Initialization	Random sampling	LR Schedule	SSRS, $\zeta = 2$ Augmentation
$\alpha_{BN}$	0.01	RandomResizedCrop RandomHorizontalFlip CutMix	

Table 10. Hyperparameter settings for ImageNet-21K.

IPC	Method	Evaluation model			
		DeiT-Tiny	Swin-Tiny	ConvNeXt-Tiny	ViT-Small
10	RDED	14.0	29.2	48.3	-
	EDC	18.4	38.3	54.4	14.9
	Ours <sub>10×</sub>	<b>23.6</b>	<b>42.7</b>	<b>55.0</b>	<b>19.8</b>
50	RDED	44.5	56.9	65.4	-
	EDC	55.0	63.3	66.6	54.5
	Ours <sub>10×</sub>	<b>56.1</b>	<b>64.3</b>	<b>66.8</b>	<b>60.7</b>

Table 11. Cross-architecture generalization on ImageNet-1K.

Method	IPC = 10		IPC = 50	
	w/o SSRS	w/ SSRS	w/o SSRS	w/ SSRS
Ours <sub>10×</sub>	$49.7 \pm 0.2$	<b><math>50.0 \pm 0.1</math></b>	$58.4 \pm 0.1$	<b><math>58.9 \pm 0.1</math></b>
Ours <sub>20×</sub>	$49.4 \pm 0.2$	<b><math>49.9 \pm 0.1</math></b>	$58.0 \pm 0.2$	<b><math>58.8 \pm 0.04</math></b>

Table 12. Ablation study on the effect of Early Smoothing-later Steep Learning Rate Schedule (SSRS) under different acceleration factors on ImageNet-1K. SSRS consistently improves performance and accelerates convergence across both IPC = 10 and IPC = 50.

of-the-art baselines on ImageNet-1K. Our synthetic representations occupy a broader region of the embedding space, indicating higher diversity and stronger generalization. At

	Run 1	Run 2	Run 3
Ours <sub>10×</sub>	10.89	12.29	12.90

Table 13. Performance across three independent runs of our method with different RDED initialization seeds on ImageNet-1K at IPC = 1 using a ResNet-18 architecture.

Method	IPC	
	10	50
EDC	44.5	57.1
Ours	<b>47.9</b>	<b>58.4</b>

Table 14. **Effect of initialization strategy.** Accuracy on ImageNet-1K when comparing the patch-based initialization of EDC with the full-image initialization adopted in our method (E<sup>2</sup>D) across two IPC settings.

the same time, class-specific clusters remain clearly separated, reflecting preserved discriminability and semantically coherent structure. These observations show that our method generates synthetic data that is diverse and semantically aligned with class structure.

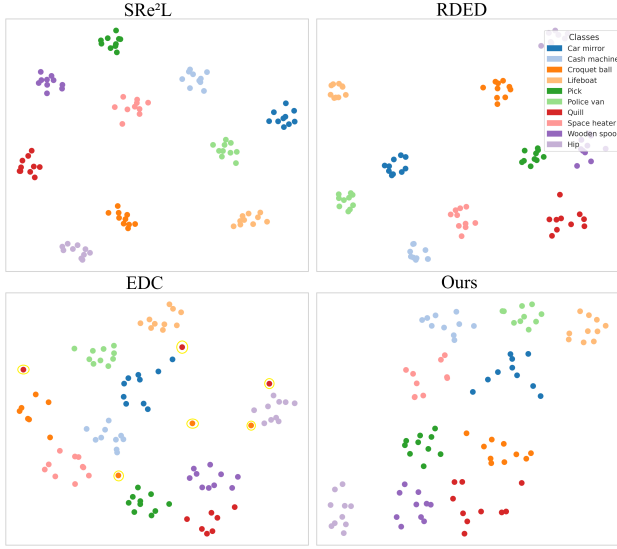


Figure 7. t-SNE visualization of logit embeddings for synthetic data generated by our method and state-of-the-art baselines on ImageNet-1K. Our method exhibits broader dispersion and clearer clusters, indicating better generalization and stronger class separability. Outlier points outside class clusters are highlighted by yellow circles.

#### Acceleration on Low-Resolution Datasets.

We exclude low-resolution datasets such as CIFAR-10 and CIFAR-100 from our primary focus, as EDC already achieves peak performance with minimal optimization, rendering further acceleration unnecessary. Table 15 examines the effect of optimization iterations on CIFAR-100 using EDC. Although the default configuration uses 2000 iterations, our findings show that omitting optimization entirely preserves final accuracy for both  $IPC = 10$  and  $IPC = 50$  without noticeable degradation. This suggests that, for low-resolution datasets, the knowledge distillation process embedded in the relabeling stage alone effectively drives performance, making extra optimization of synthetic data redundant. Similarly, for CIFAR-10, the default EDC configuration uses only 75 optimization steps, a setting that does not benefit from further acceleration.

Method	IPC 10	IPC 50
<i>EDC (reported)</i>	$63.7 \pm 0.3$	$68.6 \pm 0.2$
<i>EDC (reproduced)</i>		
No optimization	$65.1 \pm 0.2$	$68.5 \pm 0.2$
With optimization	$65.2 \pm 0.1$	$68.8 \pm 0.2$

Table 15. **Effect of optimization iterations in EDC on CIFAR-100.** The top row reports the value from the original paper; the last two rows are our reproduced results. Final accuracy remains stable even without optimization, indicating that the relabeling stage alone suffices for low-resolution datasets.

## 7. Implementation Details

### Loss Threshold

The threshold  $\epsilon$  specifies the minimum loss during exploration stage that a crop must reach to be selected for exploitation in our method. Conceptually,  $\epsilon$  acts as a filter that identifies which regions of the synthetic image provide sufficiently strong supervisory signal to justify further optimization. The threshold controls the trade-off between optimization duration and computational overhead. Lower values increase the number of retained crops, which raises computational cost, while higher values risk premature stopping, leading to suboptimal optimization. Empirically, we found that  $\epsilon = 0.5$  is effective for ImageNet-1K and  $\epsilon = 0.3$  for ImageNet-21K.

### Hyperparameter Settings

We report the hyperparameters used for each dataset experiment to facilitate reproducibility. Table 9 lists the configuration for ImageNet-1K, while Table 10 shows the settings for ImageNet-21K.

## 8. Additional Visualization

We present additional visualizations of the synthetic data generated by our method for ImageNet-1K and ImageNet-21K. By relying on full-size feature representations, our method avoids the distortions arising from spatially compressed features and produces images with higher structural fidelity and clearer class-specific patterns. Illustrative examples for ImageNet-1K are shown in Fig. 8, while corresponding ImageNet-21K examples are provided in Fig. 9.

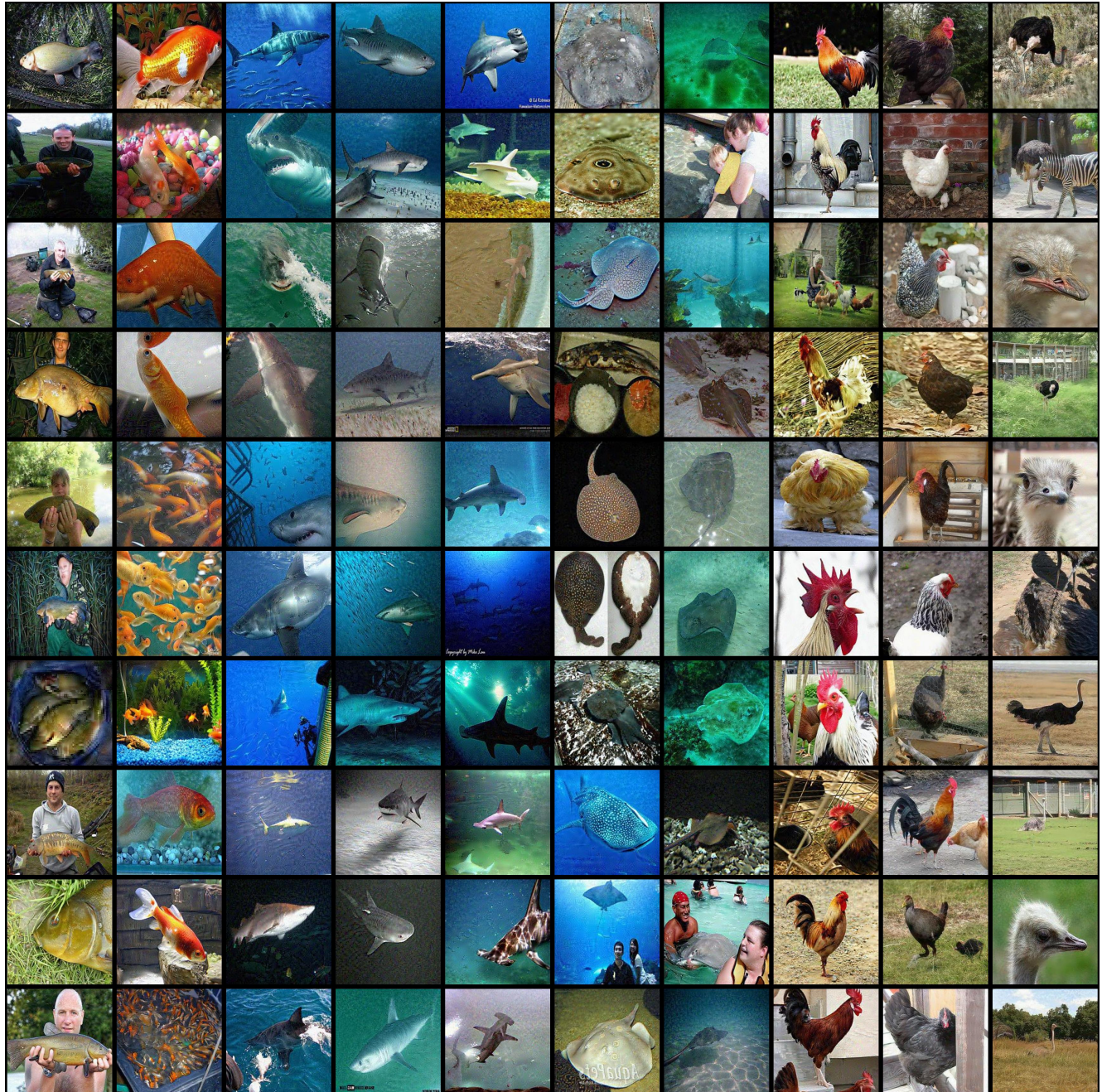


Figure 8. Visualization of synthetic images produced by our method on ImageNet-1K.

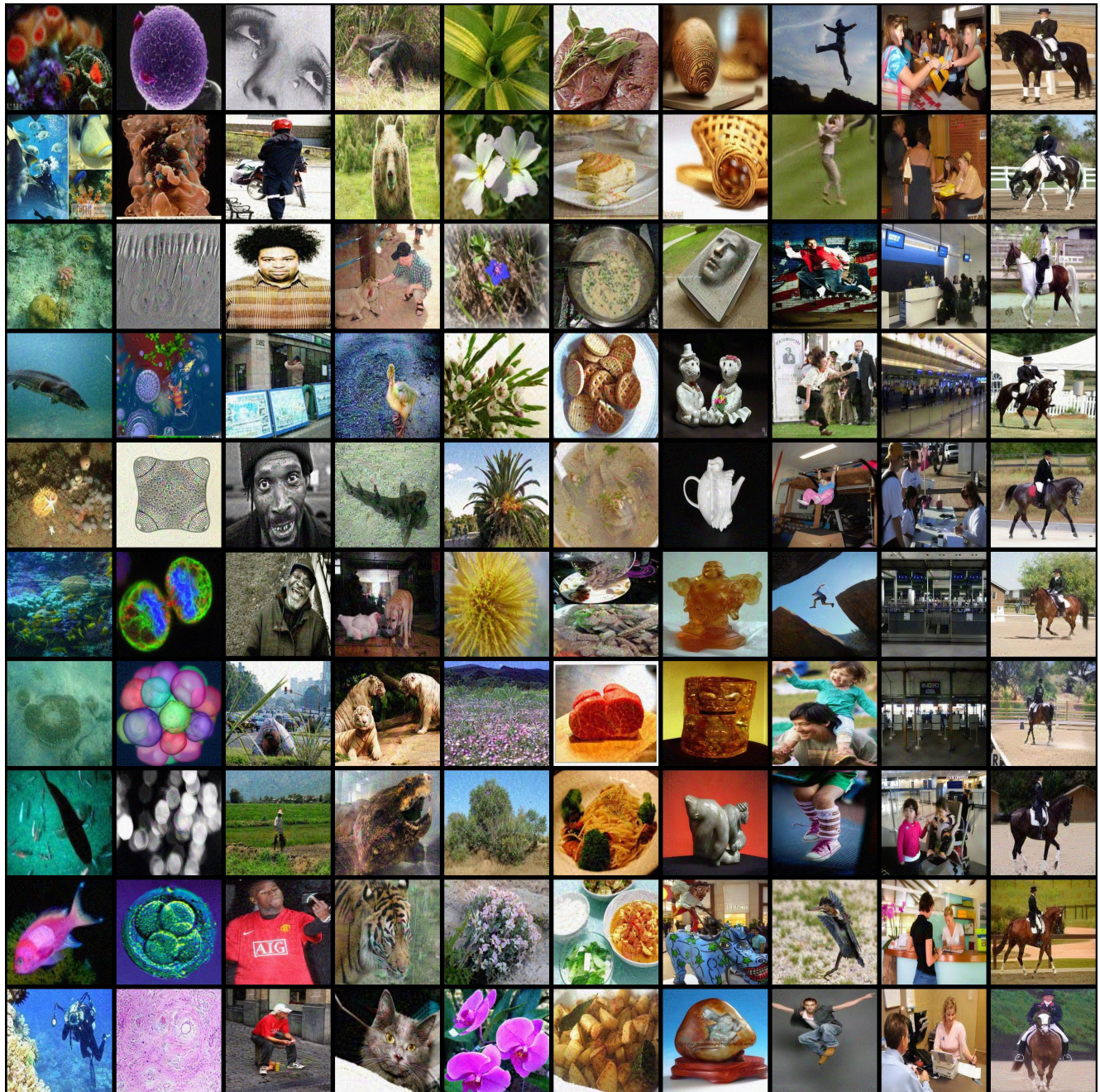


Figure 9. Visualization of synthetic images produced by our method on ImageNet-21K.